AIAA JOURNAL
Vol. 44, No. 6, June 2006

Structure of Underexpanded Jets from Square Nozzles

Seiji Tsutsumi,* Susumu Teramoto,† Kazuo Yamaguchi,‡ and Toshio Nagashima§
University of Tokyo, Tokyo 113-8656, Japan

The structure of underexpanded jets issuing from nozzles with square outlets is investigated numerically and experimentally. This type of nozzle is of interest for its use in the clustered combustors of linear aerospike engines. The numerical results indicate that the first shock cell is composed of two types of shock waves; intercepting shock waves corresponding to the oblique shock wave observed in underexpanded jets from two-dimensional planar nozzles, and recompression shock waves that appear downstream of the overexpanded regions. The overexpanded regions are formed by the interaction of expansion fans generated at neighboring nozzle edges. It is shown that the jet expands almost two-dimensionally on the symmetry planes, whereas shock waves suppress expansion on the diagonal planes, resulting in a cross shaped jet cross section.

Nomenclature

A	=	cross-sectional area
D_t	=	diameter of throat
M	=	Mach number
NPR	=	nozzle total pressure ratio (P_0/P_a)
NPR_e	=	nozzle exit static pressure ratio (P_e/P_a)
P	=	pressure
X	=	axial distance from nozzle exit plane
κ	=	specific heat ratio

Subscripts

a	=	ambient
e	=	nozzle exit plane
t	=	throat
0	=	nozzle inlet stagnation condition

Introduction

THE linear aerospike engine generally exhibits better performance over a wider altitude range than conventional rocket engines with bell nozzles.[1–3] The engine consists of a linear aerospike nozzle with combustors attached to the nozzle inlet. The combustors, or thrust cells, are clustered in lines along the inlet and are designed to have a rectangular exit so as to minimize intercell gaps. The underexpanded jets issuing from adjacent thrust cells interact to form a complicated flowfield over the linear aerospike nozzle. Hagemann et al. pointed out that the interaction causes performance losses of a few percent.[3] Many studies have been performed to investigate the loss mechanism for clustered thrust cells,[4–6] and the flow structure on the clustered aerospike nozzle and overall nozzle performance have been discussed. The flowfield over the aerospike nozzle is characterized by four features: 1) a jet structure governed by the rectangular exit of the thrust cell, 2) interaction between neighboring jets, 3) inviscid interaction between the jet and the aerospike nozzle, and 4) viscous-inviscid interaction between the jet and the nozzle surface. These features interact in a complex manner, yet the flowfield has generally been discussed without distinguishing between these features. The analysis of each feature separately can therefore be expected to provide a better understanding of the loss mechanism. The present study thus focuses on the structure of individual jets issuing from rectangular thrust cells.

Slightly underexpanded rectangular jets have been studied extensively, primarily in connection with noise suppression or thrust vector control for jet engines. Such jets have also been studied with respect to passive mixing.[7] However, there are only few reports focusing on rectangular jets at high pressure ratios, which are typical for rocket engines. Teshima studied the structure of underexpanded jets from sonic orifices at high pressure ratios by laser-induced fluorescence[8,9] and found that the expansion of these jets is not isotropic. The jets expand most prominently in the major and minor axial directions, resulting in a cross-shaped cross section. Although this characteristic should be correlated in some way with the shock-wave structure, Teshima only discussed the cross-sectional jet shape. Thus, the three-dimensional shock structure and its correlation with the jet boundary are as yet not fully understood. As such knowledge is essential for understanding the interactive flowfields on the linear aerospike nozzle, the present study through numerical and experimental analyses aims to determine the detailed flow structure of underexpanded jets issuing from a nozzle with a square exit (representative of a thrust cell). The analysis focuses on the shock structure and its correlation with the jet shape by applying shock-capturing methods to the numerical results.

Nozzle Geometry and Conditions

The nozzle studied in this report has a circular throat and a square exit, with D_t of 6 mm and nozzle wall thickness of 1.5 mm. The area ratio (A_e/A_t) is set at 2.0, giving an exit Mach number of 2.2 assuming quasi-one-dimensional flow of gaseous nitrogen ($\kappa = 1.4$). The square nozzle is carefully designed for uniform outflow, and the distribution of Mach number in the numerical analysis is less than $\pm 3\%$. As an experimental nozzle with these parameters was found to produce the same fundamental jet structures as a numerical model of an ideal nozzle with uniform outflow, only the results for uniform and parallel inflow conditions with $M_e = 2.2$ at the nozzle exit are presented in this report.

The flow conditions are listed in Table 1. The structure of the jet was investigated numerically and experimentally for a relatively low pressure ratio of $\text{NPR}_e = 2.5$. However, numerical results for two cases of NPR_e are also presented to clarify the effect of the pressure ratio.

Experimental Setup

A cold-gas blowdown test stand was used for the jet-visualization experiments. Dry, unheated gaseous nitrogen was supplied from high-pressure cylinders (15 MPa, 1.2 m^3) into a settling chamber

Received 20 August 2004; revision received 17 November 2005; accepted for publication 17 January 2006.

*Graduate Student, Department of Aeronautics and Astronautics, 7-3-1 Hongo, Bunkyo-ku.; seiji@thermo.t.u-tokyo.ac.jp. Student Member AIAA.

†Lecturer, Department of Aeronautics and Astronautics, 7-3-1 Hongo, Bunkyo-ku. Member AIAA.

‡Research Associate, Department of Aeronautics and Astronautics, 7-3-1 Hongo, Bunkyo-ku.

§Professor, Department of Aeronautics and Astronautics, 7-3-1 Hongo, Bunkyo-ku. Member AIAA.

via a pressure regulator. A particle mixer was inserted upstream of the settling chamber to mix the main flow with the particles for flow visualization. The test nozzle was mounted on the settling chamber and then placed in the test chamber. A supersonic diffuser was installed at the exit of the test chamber to achieve a higher pressure ratio.

The planar Mie scattering method was employed to visualize the cross sections of the jet. Solid particles with a nominal diameter of 2.0 μm and density of 3 g/cm^3 were used as scattering particles. A He–Ne laser (30 mW, 632.8-nm wavelength) was employed as a light source, and scattering images were taken using a digital video camera at a frame rate of 1/30 s.

Numerical Analysis

Numerical Method

The governing equations employed for the numerical analysis were the Reynolds-averaged unsteady three-dimensional thin-layer Navier–Stokes equations.

Numerical fluxes for the convective terms were evaluated by the simple high-resolution upwind scheme (SHUS),[10] which is a family of advection upwind splitting method (AUSM) type schemes. Second-order spatial accuracy was obtained by adopting monotonic upwind schemes for conservation laws (MUSCL) interpolation based on the primitive variables. The lower-upper alternating-direction-implicit (LU-ADI) algorithm[11] was employed for time integration.

The computational code employed for analysis is based on the in-house code developed by the Japan Aerospace Exploration Agency. This code has been applied for a wide variety of flowfields and has been extensively validated.[4,12] Discussions on the detail and accuracy of the computational code can be found in the literature.

Assuming symmetry, only one-quarter of the flowfield was simulated. The fine H-grid is located in the area where the target jet structure appears, and the region outside this inner region is covered by the C-grid. As cases with high pressure ratio require fine-grid resolution near the lip, the total number of grid points differs from case to case, as shown in Table 1.

Table 1 Flow conditions

NPR_e	NPR	Grid number
1.38	14.76	753,645
2.5	26.7	753,645
7.5	80.2	1,377,935

Postprocessing

The shock-wave structure is considered to be the key factor determining the expansion of the supersonic jet. Thus, visualization of the shock surface is very useful for understanding the flowfield. Two approaches have been proposed for identification of the shock surface in numerical results. One approach is based on the normal Mach number M_n, which is the Mach-number component in the direction of the gradient of a scalar quantity. The shock is considered to be located at the point where the normal Mach number is equal to one.[13–15]

The other method employs a directional derivative, which is the derivative of a scalar quantity in the direction of the local velocity vector. The position of the shock surface is assumed to be located at the point where the second directional derivative is equal to zero for nonzero first directional derivative. This method is described in detail in the literature.[15,16]

In the present study, M_n is evaluated from the gradient of the velocity magnitude. The filtering technique proposed by Cebral and Löhner[14] is used to filter out physically irrelevant normal vectors. This method is applied to the higher pressure ratio examined here ($NPR_e = 7.5$). The directional derivative of static pressure is computed for visualization of the shock surface at the lower pressure ratio ($NPR_e = 2.5$). As the flowfield considered in this study is essentially unsteady, the flow structure is discussed based on time-averaged properties.

General Features of Underexpanded Jet Structure for $NPR_e = 2.5$

Figures 1 and 2 compare the Mie scattering images for $NPR_e = 2.56$ ($NPR = 27.38$) with numerical density contours for $NPR_e = 2.5$. The numerical results for $NPR_e = 2.56$ were also considered, but the difference is negligible, and those results are omitted for consistency. Although it is inappropriate to compare these figures directly, because the figures visualize different physical properties, the numerical and experimental results both reproduce the key features

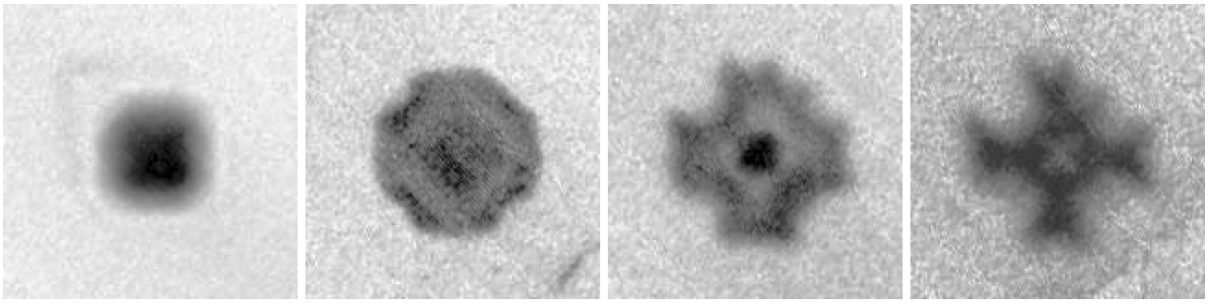

Fig. 1 Mie scattering images of jet cross sections for $NPR_e = 2.56$ (NPR = 27.38).

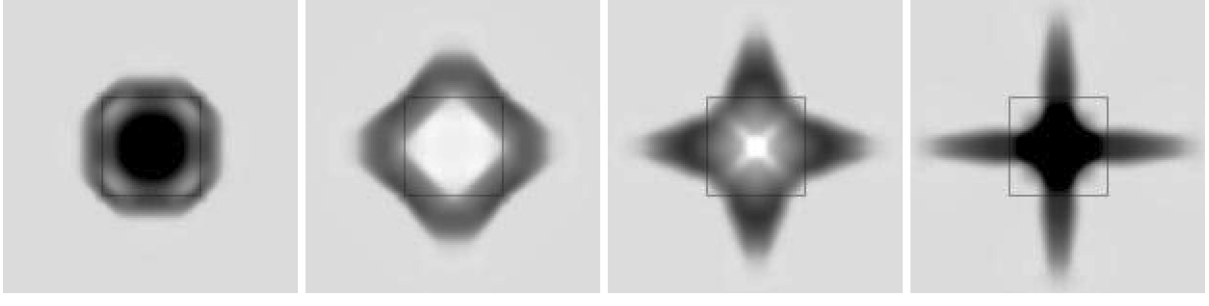

Fig. 2 Numerical density contour of jet cross sections for $NPR_e = 2.5$.

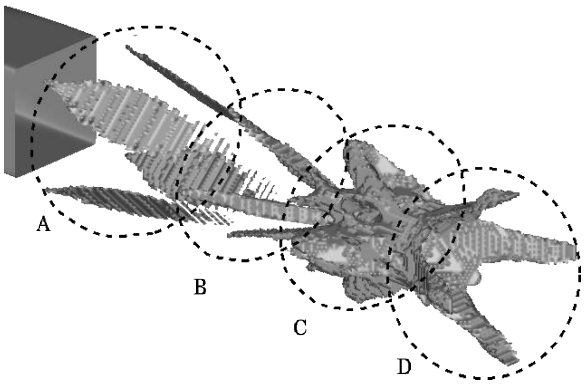

Fig. 3 Shock surface.

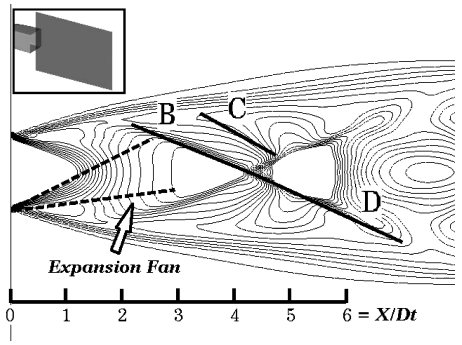

a) Symmetry plane

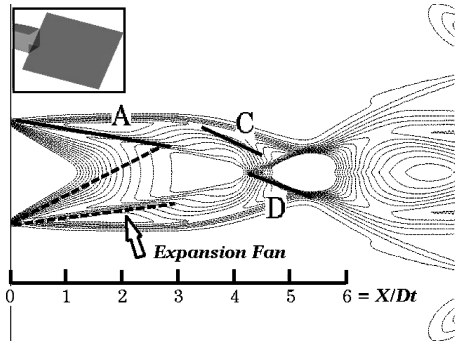

b) Diagonal plane

Fig. 4 Schematics of flow structure on symmetry and diagonal planes.

reported by Teshima,[8,9] and the comparison is in general satisfactory. The minor discrepancy at $X/D_t = 4.2$ and 5.8 is mainly attributable to poor traceability of the scattering particles. The jet expands outward on the vertical and horizontal symmetry planes, yet does not expand significantly on the diagonal planes. As a result, the jet forms a cross-shaped cross section.

This cross-like jet shape differs considerably from the shape of jets issuing from axisymmetric nozzles. Figure 3 shows the shock surface. The shock surfaces are classified into four categories (A–D). Shock surfaces A appear at the four corners of the nozzle exit and disappear downstream at approximately $X/D_t = 2.8$, where shock surfaces B emerge on the vertical and horizontal symmetry planes. Shock surfaces B are inclined toward the centerline. Shock waves C are more complex, but it can be observed that the shock surfaces emerge on the symmetry and diagonal planes. Finally, shock waves D, consisting of four shock surfaces, appear on the symmetry planes. These shock structures are each described in detail next.

Shock-Wave Structure

Figure 4 shows the density contours on the symmetry and diagonal planes. On the symmetry plane, an oblique shock wave B forms at approximately $X/D_t = 2.0$ and intersects regularly at $X/D_t = 4.2$.

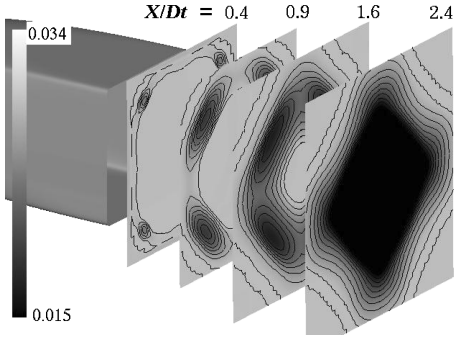

Fig. 5 Cross-sectional static-pressure distribution.

On the diagonal plane, shock waves A appear immediately downstream of the nozzle exit. The oblique shock waves are generated upstream of the intersection of the expansion fans and the jet boundary. Therefore, it is clear that shock waves A and B do not represent "intercepting shock waves," which is a shock wave formed by the coalescence of compression waves caused by expansion fan reflected at jet boundary. Figure 5 shows the static-pressure distributions at four distances from the outlet. Overexpanded regions appear near the four corners at $X/D_t = 0.4$ and 0.9. Comparing Figs. 3 and 5, the shock waves A coincide with the outer edges of these overexpanded regions. Prandtl–Meyer expansion fans are generated from each edge of the square nozzle outlet, and the expansion fans from neighboring nozzle edges interact in the corner regions, resulting in overexpanded flow. It is observed from Fig. 5 that the static pressure in those overexpanded regions is lower than the ambient pressure, resulting in the formation of recompression shock waves to recover the static pressure. Shock wave A shown in Figs. 3 and 4b corresponds to this recompression shock wave.

As the jet flows downstream, the overexpanded regions shown in Fig. 5 grow and eventually merge at $X/D_t = 1.6$, causing another recompression shock wave B to emerge on the symmetry planes. Therefore, shock wave B also represents a recompression shock wave formed behind the intersection of neighboring overexpanded regions.

It is observed from Fig. 4 that shock waves C are generated at about $X/D_t = 3.3$ on both the symmetry and diagonal planes. The Mach angles of the head and tail of the expansion fan are 27.0 and 7.2 deg, respectively. The generation point for shock waves C roughly coincides with the intersection between the head of the expansion wave and the jet boundary. Thus, shock wave C is considered to represent an intercepting shock wave.

Finally, shock wave D on the symmetry plane is in fact the recompression shock wave B after the regular intersection. Shock wave D on the diagonal plane (Fig. 4b) also appears to be the recompression shock wave A after the regular intersection. However, shock wave A in the range $X/D_t = 2.8$ to 4.2 is so weak that the present shock-detection algorithm does not recognize the pressure gradient in this region as a shock wave. Thus, shock wave A disappears at $X/D_t = 2.8$ in Fig. 3. The expansion fans issuing from the nozzle edges meet shock waves A, representing the main cause of attenuation of the A-type shock waves in this region. The recompression shock waves D extend to the jet boundary. As the jet is much wider in the symmetry plane than in the diagonal plane (see Fig. 4), the recompression shock wave extends outward much farther on the symmetry plane.

Correlation Between Shock Wave and Jet Boundary

As shown in Fig. 2, the cross shape of the jet cross section originates from the difference between jet expansion in the symmetry and diagonal planes. The jet boundary on the symmetry plane (Fig. 4a) expands straight outward at approximately 14.0 deg, in agreement with the angle evaluated from Prandtl–Meyer theory. The recompression shock wave B appears to have little influence on the jet boundary. Shock wave B is a recompression shock wave caused by intersection of the overexpanded regions and is not produced by reflection of the expansion fan from the jet boundary. Therefore,

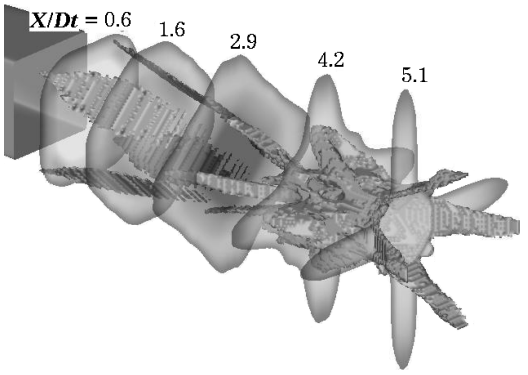

Fig. 6 Shock surface with density contours showing jet boundary.

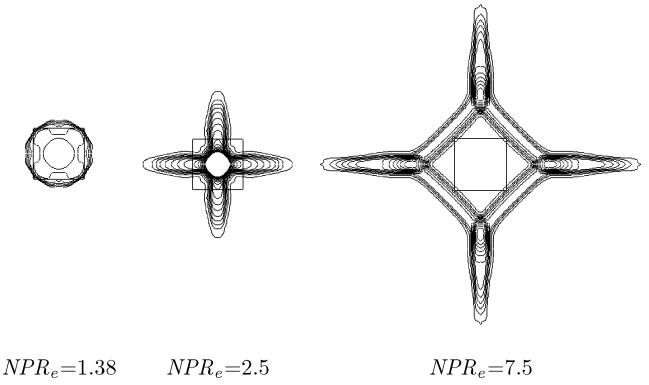

Fig. 7 Comparison of representative cross sections.

shock wave B does not influence the jet boundary. The jet boundary on the symmetry plane does not encounter compression waves until $X/D_t \simeq 3.0$ and thus expands linearly within this region. However, the jet boundary on the diagonal plane (Fig. 4b) passes through the recompression shock wave A immediately downstream of the intersection with the expansion fan, causing it to turn inward. Downstream, the jet boundary on the diagonal plane turns further inward at about $X/D_t = 3.3$ as a result of the intercepting shock wave C, which also appears on the symmetry plane although its effect is weak. Finally, the first shock cell ends as the jet boundary meets the recompression shock waves D.

The preceding discussions focus mainly on the two-dimensional view of the flowfield. Figure 6 shows the three-dimensional shock surface with density contours at five cross sections. Each cross section is displayed only for the region in which the normalized pitot pressure is higher than 0.08 (indicating the jet boundary). Figure 6 clearly reveals the correlation between the shock waves and the jet boundary. The four corners of the jet boundary are gradually flattened from $X/D_t = 0.6$ to 2.9, and the shape of the cross sections changes from an upstream square to an octagon, and finally to a square inclined by 45 deg. The width of the flattened part of the jet at $X/D_t = 0.6$ and 1.6 is in agreement with the width of the recompression shock wave A. As the recompression shock wave A turns the flow inward, the flattening on the diagonal planes can be related directly to shock wave A. Another series of recompression shock waves (group B) also appears on the symmetry planes. These waves B turn the flow inward, but do not intersect with the jet boundary. Thus the recompression shock wave B does not influence the jet shape, and the jet boundary on the symmetry planes continues to expand outward. At $X/D_t = 4.2$, the jet boundaries on the diagonal planes meet shock waves C and turn further inward. Although the effect is not as prominent as for shock wave A, the difference in the expansion of the jet boundary between the symmetry planes and the diagonal planes becomes substantial, and a clear cross-shaped cross section is formed at $X/D_t = 5.1$.

Effect of Pressure Ratio Changes

Figure 7 compares representative density cross sections of the jet for three different pressure ratios. It is clear that the pressure ratio affects the jet shape. At the lowest pressure ratio ($\mathrm{NPR}_e = 1.38$), the cross section deforms only slightly. However, the cross shape becomes more distinct with increasing pressure ratio. In the case of $\mathrm{NPR}_e = 7.5$, the cross section has a diamond shape, and the expansion on the symmetry planes is remarkable.

The small deformation at $\mathrm{NPR}_e = 1.38$ is caused by the weaker nature of the expansion fans and shock waves, which have little effect on the jet boundary. However, the strength of the expansion fans and shock waves alone does not explain the transition from the simple cross shape to the diamond shape for the case of $\mathrm{NPR}_e = 7.5$. Figure 8 shows the shock surface and cross-sectional density contours for $\mathrm{NPR}_e = 7.5$. The threshold based on the pitot pressure is also applied to indicate the jet boundary. Recompression shock waves A and B are formed at the corners of the nozzle exit and on the symmetry planes. Intercepting shock waves C also appear at approximately $X/D_t = 3.5$. The intercepting shock is so wide that it covers the entire flowfield between recompression shock waves B.

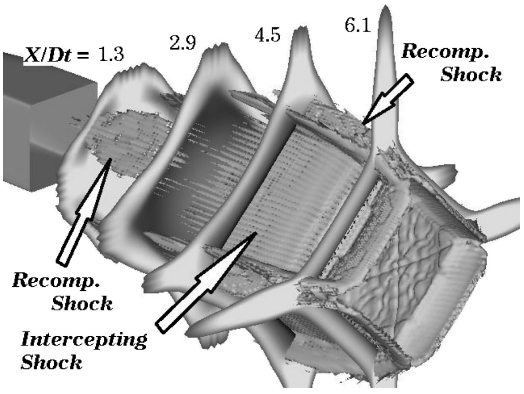

Fig. 8 Shock surface and jet boundary for $\mathrm{NPR}_e = 7.5$.

The central angle of the expansion fan from the nozzle edge changes according to the pressure ratio. The angle is estimated to be 38.0 deg for $\mathrm{NPR}_e = 7.5$ and 19.9 deg for $\mathrm{NPR}_e = 2.5$. The larger central angle of the expansion fan has two effects on the shock structure; a larger overexpanded region is produced at the corners, which results in a wider recompression shock wave A, and the fan spreads wider in the flowfield. According to this shock structure, the flattened part of the jet boundary at the four corners widens, and the narrow limbs of the jet on the symmetry planes extends outward two dimensionally. Downstream, the jet boundaries at the corners meet the intercepting shock waves and turn further inward, resulting in a remarkable difference in expansion between the symmetry planes and the diagonal planes.

Conclusions

Underexpanded jets from a square nozzle were studied numerically and experimentally. Numerical analysis revealed that the shock structure inside the underexpanded jet consists of recompression shock waves and intercepting shock waves, the latter of which correspond to the shock observed in underexpanded jets issuing from two-dimensional planar nozzles. A recompression shock wave is generated downstream of the overexpanded regions at the corners of the nozzle outlet through interaction between adjacent expansion fans. The overexpanded regions grow downstream and eventually join on the symmetry planes, generating another recompression shock wave.

The resultant shape of the jet is determined by these shock waves. The jet expands two dimensionally on the symmetry planes through Prandtl–Meyer expansion fans from the nozzle edges. At the corners of the flow, the jet turns inward as a result of the effect of recompression shock waves and intercepting shock waves. These flow and interaction features result in a jet with a cross-shaped cross section.

The shock structure at higher pressure ratios is also characterized by intercepting shock waves and recompression shock waves. However, the recompression shock waves at the corners of the nozzle

flow become wider with increasing pressure ratio, and the intercepting shock waves spread wider in the flowfield. As a result, the cross-sectional jet becomes more diamond shaped with increasing pressure ratio.

These features were confirmed experimentally. The cross-sectional jet shape visualized by the planar Mie scattering method also revealed a clear cross shape.

This study not only revealed the detail flow structure, but also demonstrated the usefulness of the shock-capturing method for analyzing complex three-dimensional shock structures. These results are helpful for discussing flowfields with three-dimensional shock waves such as those produced by aerospike nozzles and can contribute to identifying the causes of performance loss in clustered thrust cells.

References

[1]Sutton, G. P., and Biblarz, O., *Rocket Propulsion Elements*, 7th ed., Wiley-Interscience, New York, 2001, pp. 296–300.

[2]Ruf, J. H., and McConnaughey, P. K., "The Plume Physics Behind Aerospike Nozzle Altitude Compensation and Slipstream Effect," AIAA Paper 97-3218, July 1997.

[3]Hagemann, G., Immich, H., and Dumnov, G., "Critical Assessment of the Linear Plug Nozzle Concept," AIAA Paper 2001-3683, July 2001.

[4]Ito, T., and Fujii, K., "Flow Field and Performance Analysis of the Simplified Clustered Aerospike Nozzles," AIAA Paper 2001-2861, June 2001.

[5]Tomita, T., Takahashi, M., and Tamura, H., "Flow Field of Clustered Plug Nozzles," AIAA Paper 97-3219, July 1997.

[6]Nasuti, F., and Geron, M., and Paciorri, R., "Three Dimensional Features of Clustered Plug Nozzle Flows," AIAA Paper 2003-4910, July 2003.

[7]Gutmark, E. J., and Grinstein, F. F., "Flow Control with Noncircular Jets," *Annual Review of Fluid Mechanics*, Vol. 31, 1999, pp. 239–272.

[8]Teshima, K., "Two-Dimensional Focusing of a Supersonic Free Jet by a Rectangular Orifices," *Physics of Fluids*, Vol. 30, No. 7, 1987, pp. 1899–1901.

[9]Teshima, K., "Three-Dimensional Characteristics of Supersonic Jets," *Proceedings of the 17th International Symposium on Rarefied Gas Dynamics*, edited by A. E. Beylich, VCH Verlagsgesellschaft mbH, Weinheim, Germany, 1990, pp. 1042–1048.

[10]Shima, E., and Jounouchi, T., "Role of CFD in Aeronautical Engineering (No. 14) - AUSM Type Upwind Schemes," *Proceedings of the 14th NAL Symposium on Aircraft Computational Aerodynamics*, NAL SP-34, National Aerospace Lab., Tokyo, 1997, pp. 7–12.

[11]Obayashi, S., Matsushima, K., Fujii, K., and Kuwahara, K., "Improvements in Efficiency and Reliability for Navier–Stokes Computations Using the LU-ADI Factorization Algorithm," AIAA Paper 86-0338, Jan. 1986.

[12]Fujii, K., and Obayashi, S., "Navier–Stokes Simulations of Transonic Flows over a Practical Wing Configuration," *AIAA Journal*, Vol. 25, No. 3, 1987, pp. 369, 370.

[13]Lovely, D., and Haimes, R., "Shock Detection from Computational Fluid Dynamics Results," AIAA Paper 99-3285, June 1999.

[14]Cebral, J., and Löhner, R., "Visualization on Unstructured Grids Using Geometrical Cuts, Vortex Detection and Shock Surfaces," AIAA Paper 2001-0915, Jan. 2001.

[15]Ma, K., Rosendale, J., and Vermeer, W., "3D Shock Wave Visualization on Unstructured Grids," *Proceedings of 1996 Symposium on Volume Visualization*, Inst. of Electrical and Electronics Engineers, 1996, pp. 87–94.

[16]Pagendarm, H., and Seitz, B., "An Algorithm for Detection and Visualization of Discontinuities in Scientific Data Fields Applied to Flow Data with Shock Waves," *Scientific Visualization—Advanced Software Techniques*, Ellis Horwood, New York, 1993, pp. 161–177.

K. Ghia
Associate Editor